

Dynamical effects of long-range interaction revealed in screened Coulomb interacting ring systems

Zhenwei Yao*

*School of Physics and Astronomy, and Institute of Natural Sciences,
Shanghai Jiao Tong University, Shanghai 200240, China*

Understanding the intriguing physical effects of long-range interactions is a common theme in a host of physical systems. In this work, based on the classical screened Coulomb interacting ring model, we investigate the dynamical effects of the long-range interaction from the unique perspective of analyzing the dynamical response of the system to disturbance. We reveal the featured dynamics brought by the long-range interaction, including the efficient transformation of the disturbance into the uniform global rotation of the system, the suppression of the intrinsic noise, and the fast relaxation of particle speed.

I. INTRODUCTION

Long-range interactions are widely seen in multiple fields, ranging from astrophysics [1–3], hydrodynamics [4–6] to electrostatic and dipolar systems [7–12]. Notably, electrostatic interaction provides an important organizing force to fabricate exceedingly rich morphologies in various soft matter systems [13–18]. In long-range interacting systems, the strong coupling among the elementary constituents brings in intriguing behaviors not found in systems with short-range interactions [8, 19–22], and meanwhile imposes a grand challenge in theoretical treatment of such systems [23–25]. Understanding the dynamical effects of long-range interaction is closely related to a host of physical problems, such as the formation of long-range order [26–28] and the origin of nonlinear dynamical structures arising in various contexts [29–32]. While our knowledge about long-range interacting systems has been significantly advanced by solving kinetic equations and mean-field models, the approach based on precise numerical integration of the equations of motion has proven to be a powerful tool to reveal the fundamental microscopic dynamics not accessible by mean-field theories [32–35].

In this work, we investigate the effect of long-range interaction on the microscopic dynamics of interacting particles from the unique perspective of analyzing the dynamical response of the system to disturbance imposed on a single particle. Our model system consists of a collection of particles confined on a ring that interact by the screened Coulomb potential; this screened Coulomb interacting ring model is an invariant version of the self-gravitating ring model and may be realized in colloidal experiments [36–39]. Adopting the screened Coulomb potential, which can be experimentally realized in electrolyte solutions [40, 41], allows us to conveniently control the range of interaction, and thus highlight the unique effect of long-range interaction. Restricting the configurational space of the particles on the periodic 1D manifold excludes the subtle boundary effect. By ana-

lyzing the dynamical evolution of the system upon the disturbance, we reveal the featured dynamics driven by the long-range interaction, including the emergence of fine wave structure over the trajectory of the disturbed particle and the proliferation of dynamical modes in the energy spectrum. Long-range interaction also leads to efficient transformation of the disturbance into the uniform global rotation of the system, suppression of the intrinsic noise, and fast relaxation of particle speed.

II. MODEL AND METHOD

The model system consists of N identical point particles of mass m confined on a ring of radius R_0 , as shown in fig. 1(a). The particles are initially evenly distributed on the ring with the lattice spacing $a_0 = R_0\beta_0$, where $\beta_0 = 2\pi/N$. The collection of geometrically confined, interacting particles are treated as a pure classical mechanical system, and we work in the microcanonical ensemble with fixed number of particles and total energy. The microscopic dynamics of the particles is governed by the Hamiltonian:

$$H = \sum_{i=1}^N \frac{\vec{L}_i^2}{2mR_0^2} + \frac{1}{2} \sum_{i \neq j} V(r_{ij}), \quad (1)$$

where the screened Coulomb potential

$$V(r_{ij}) = V_0 \frac{e^{-r_{ij}/\lambda_D}}{r_{ij}}. \quad (2)$$

\vec{L}_i is the angular momentum of the particle i , r_{ij} is the Euclidean distance between particles i and j , and λ_D is the Debye screening length [40]. The range of interaction could be controlled by the screening length λ_D . Dynamics is introduced by specifying an initial velocity \vec{v}_{ini} directly to a single particle; the remaining particles are at rest. \vec{v}_{ini} is tangent to the ring, and its magnitude is Γv_0 , where v_0 is the characteristic speed. $v_0 = \sqrt{V_0/(ma_0)}$. The strength of the initial disturbance is determined by the dimensionless quantity Γ . The disturbed particle serves as a probe to reveal the dynamical effects of long-range interaction. To investigate the relaxation process,

*Electronic address: zyao@sjtu.edu.cn

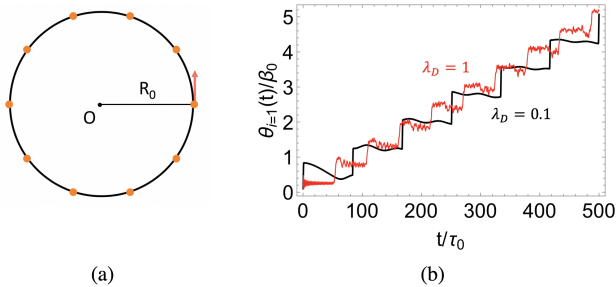


FIG. 1: Trajectories of the disturbed particle in the ring model. (a) Schematic plot of the model consisting of identical point particles confined on the ring of radius R_0 that interact by the screened Coulomb potential. (b) The trajectories of the disturbed particle (labelled as $i = 1$) for both cases of $\lambda_D = 0.1$ and $\lambda_D = 1$. The initial speed is specified by $\Gamma = 1$; see main text for more information. $N = 100$.

we also discuss the case that all the particles are disturbed. The length, mass, and time are measured in the units of the lattice spacing a_0 , particle mass m and τ_0 . $\tau_0 = a_0/v_0$.

We numerically integrate the equations of motion derived from the Hamiltonian in eq.(1) for long-time (up to hundreds of times of the characteristic time scale) trajectories of motion at high precision. The time step h is set to be sufficiently fine to ensure that during a hundred million simulation steps the variations of the total energy and the angular momentum are within one thousandth with respect to the mean kinetic energy and the mean angular momentum. Typical, $h = 10^{-5}\tau_0$. No cut-off length is introduced in dealing with the long-range interaction between particles. We investigate the dynamical and statistical effects of long-range interaction by analyzing the energy spectra and some key dynamical parameters.

III. RESULTS AND DISCUSSION

A. Energy spectral analysis

We first track the motion of the disturbed particle labelled as $i = 1$. The recorded trajectory $\theta_{i=1}(t)$ is presented in fig. 1(b); the value for $\theta_{i=1}(t)$ is scaled by the initial particle-particle angular distance β_0 to show the relative displacement of the particles. It clearly shows that varying the range of interaction from $\lambda_D = 0.1$ to $\lambda_D = 1$ leads to distinct behaviors of the disturbed particle. The displacement curve (black) in fig. 1(b) for $\lambda_D = 0.1$ exhibits stepped feature. Each fast forward motion with the abrupt increase of θ is accompanied by a very slow backward motion. This featured rhythm in the motion of the disturbed particle persists during the entire simulation time of $\Delta t = 500\tau_0$. In the strong screening regime of small λ_D , the interaction of adjacent parti-

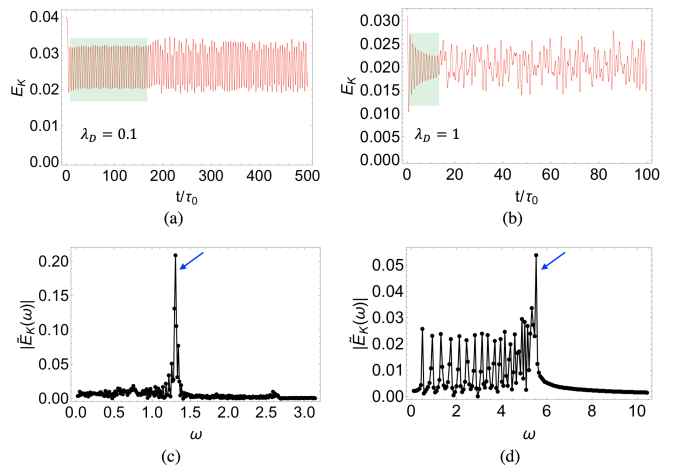


FIG. 2: Spectral analysis of the kinetic energy of short- and long-range interacting systems. The spectral analysis is based on 5000 recorded energy data. The spectra of the kinetic energy curves in (a) and (b) for $\lambda_D = 0.1$ and $\lambda_D = 1$ are presented in (c) and (d), respectively. More dynamical modes are excited in the latter system. The peak frequencies indicated by the arrows correspond to the initial regular oscillations in the green regions in (a) and (b). The energy is measured in the unit of $\epsilon_0 = m(a_0/\tau_0)^2$. $\Gamma = 0.1$. $N = 50$.

cles resembles the two-body collision in Newton's cradle, and it is thus expected that the steps in the displacement curve of the disturbed particle would become flat. In contrast, for $\lambda_D = 1$, the motion of the disturbed particle is simultaneously affected by several neighboring particles, resulting in the fine wave structure in the trajectory as shown in the red curve in fig. 1(b). To exclude the possibility that the wave structure may be caused by any artifact arising in simulations, we vary the initial speed, the number of particles and the time step, and obtain consistent results. $\theta_{i=1}(t)$ -curves at larger screening lengths are also featured with the fine wave structure. As such, the single disturbed particle serves as a probe to reveal the subtle dynamical effect associated with the long-range nature of the interaction.

Figures 2(a) and 2(b) show the long-time kinetic energy curves for $\lambda_D = 0.1$ and $\lambda_D = 1$. A common feature of both kinetic energy curves is the sharply divided regular and irregular oscillations. The regular regions are indicated by the light green boxes. It is observed that the kinetic energy for $\lambda_D = 1$ oscillates much faster than that for $\lambda_D = 0.1$. Furthermore, the amplitude of the oscillation is significantly reduced in time for $\lambda_D = 1$. In the region of irregular oscillation, the kinetic energy curve for $\lambda_D = 1$ is subject to stronger undulations.

To uncover the underlying dynamical modes, the kinetic energy curves in figs. 2(a) and 2(b) are Fourier transformed, and the results are presented in figs. 2(c) and 2(d). The peak frequencies indicated by the arrows correspond to the initial regular oscillations in figs. 2(a) and 2(b), respectively. The energy spectra reveal a significant difference between the short- and long-range interactions:

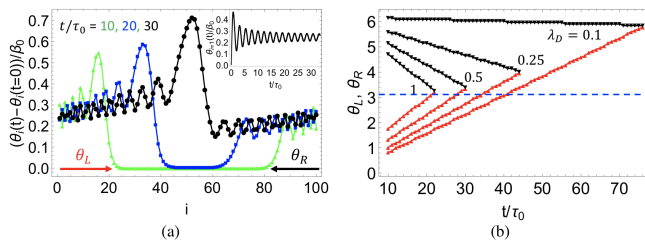


FIG. 3: Mobilization of the initially static particles triggered by the disturbed particle. (a) Temporally varying $\theta_i(t)$ profiles, where i is the label of particles in sequence around the ring. β_0 is particle-particle angular distance in the initial regular packing of the particles on the ring. The dynamics of the disturbed particle ($i = 1$) is also presented in the inset. $\lambda_D = 1$. (b) The mobilization process exhibits reflection symmetry with respect to the disturbed particle as the range of interaction increases. θ_L and θ_R represent the locations of the bilateral frontiers of the mobilized particles around the initially disturbed particle, as indicated by the arrows in (a). $N = 100$. $\Gamma = 1$.

more dynamical modes are excited in the latter system. This phenomenon shall be attributed to the enhanced nonlinearity effect under long-range interaction [42].

B. Mobilization process

To explore the physical origin of the dynamical transition from the regular to the irregular oscillation of the kinetic energy in fig. 2, we analyze the propagation of the disturbance on the single particle. Through the persistent back-and-forth interactions with neighboring particles, the initially disturbed particle mobilizes the remaining particles in sequence. A key observation is that, prior to the complete mobilization of the entire system, the variation of the total kinetic energy follows the regular pattern in fig. 2.

We further analyze the mobilization process quantitatively in terms of the two dynamical variables θ_L and θ_R whose definitions are shown in fig. 3(a). In fig. 3(a), $\theta_i(t)$ is the position of particle i at time t . θ_L and θ_R are the locations of the bilateral frontiers of the mobilized particles around the initially disturbed particle. Each curve in fig. 3(a) represents an instantaneous particle configuration. The trajectory of the initially disturbed particle is presented in the inset. Comparison of the $\theta_i(t)$ -curves at $t/\tau_0 = 10$ (green) and $t/\tau_0 = 20$ (blue) shows the movement of the frontiers of the mobilized particles as characterized by the increase of θ_L and the decrease of θ_R .

The evolution of θ_L and θ_R at varying λ_D is plotted in fig. 3(b). All of the particles are mobilized as the pair of the curves (red and black) meet at the ends. The dashed horizontal line at $\theta = \pi$ indicates the reference position of the diametrical particle with respect to the disturbed one. Figure 3(b) shows the discrepancy of the

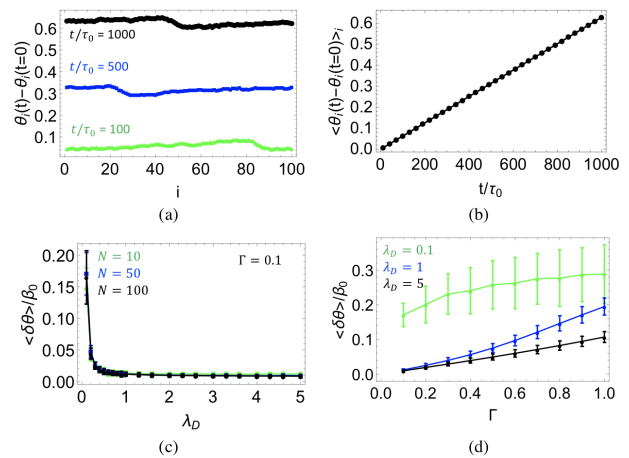


FIG. 4: Suppression of the noise in the driven motion of particles under the long-range interaction. (a) The irregularity in the profile of the particle displacement $\theta_i(t) - \theta_i(t = 0)$ indicates the presence of noise in the motion of particles. $\lambda_D = 1$. $\Gamma = 1$. (b) Plot of the mean particle displacement versus time. The averaging is over all the particles. The linear curve describes the uniform global rotation of the particles. (c) and (d) Dependence of the noise amplitude $\langle \delta\theta \rangle$ on the screening length λ_D and the initial speed Γ of the disturbed particle. $\langle \delta\theta \rangle$ is the time-averaged standard deviation of the particle displacement over twenty particle configurations from $t \in [0, 200\tau_0]$. $\Gamma = 0.1$ (c). $N = 100$ (d).

bilateral mobilization rates in the relatively short-range interacting systems. The particles towards which the disturbed particle initially approaches are mobilized in a much faster rate than those on the other side. To understand the origin of the dynamical asymmetry, we notice that the loss of the momentum of the disturbed particle in the first collision leads to a much milder second collision with the other neighbor [see the curve of $\lambda = 0.1$ in fig. 1(b)]. Here, for the long-range interacting particles on the ring, the term collision refers to the approaching and subsequent bouncing-away of two adjacent particles. The reflection symmetry around the disturbed particle is thus broken. With the increase of λ_D , the bilateral frontiers of the mobilized particles tend to advance at a common rate as shown in fig. 3(b). In other words, long-range interaction preserves the reflection symmetry in the bilateral mobilization processes around the disturbed particle. Furthermore, fig. 3(b) suggests that the entire system would be mobilized in a faster fashion with the increase of λ_D .

C. Global rotation and intrinsic noise

We further discuss the long-time collective dynamics driven by the disturbed particle. Typical instantaneous particle configurations are presented in fig. 4(a). The elevating displacement curve implies the global rotation of the particles. Note that the global rotation as charac-

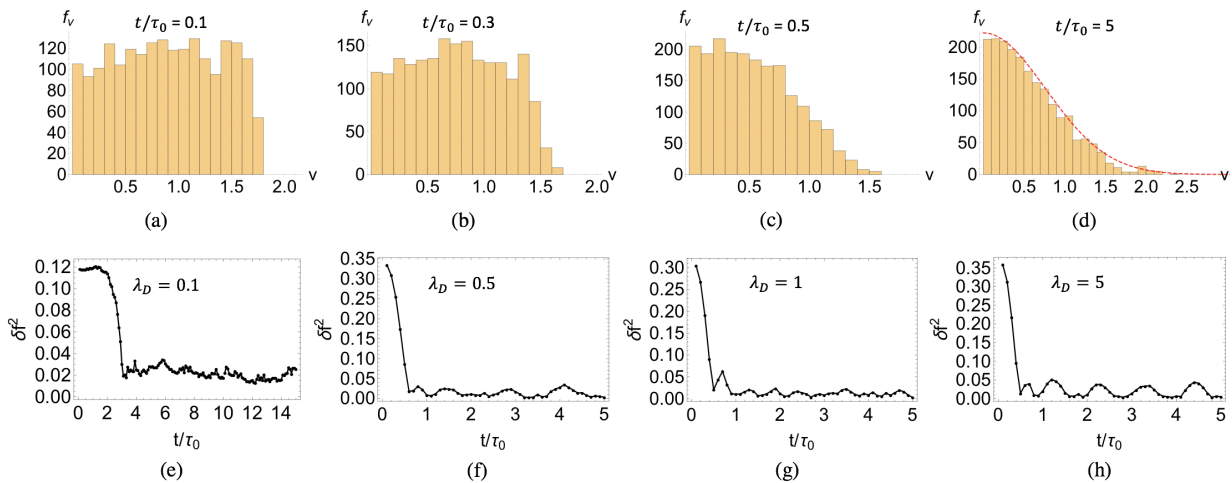


FIG. 5: Relaxation process of the particle speed. (a)-(d) Typical instantaneous speed distributions at $\lambda_D = 1$. (e)-(h) Plot of the $\delta f^2(t)$ curves at varying screening length. δf^2 is the deviation of an instantaneous speed distribution from the one-dimensional Maxwell-Boltzmann distribution. See the main text for more information. $N = 2000$. $\Gamma_m = 0.1$.

terized by the elevation of the displacement curve occurs when all particles are mobilized for $t/\tau_0 \gtrsim 55$. Such a dynamical state is characterized by the mean displacement $\langle \theta_i(t) - \theta_i(t=0) \rangle_i$ in fig. 4(b); the averaging is over all the particles. Figure 4(b) shows that the mean displacement is a linear function of time, indicating that the global rotation is uniform. The slope $\dot{\theta}_{rot}$ of the line in fig. 4(b) is determined by the initial speed of the disturbed particle. For the case in fig. 4, the relative difference between $\dot{\theta}_{rot}$ and $v_{ini}/(R_0N)$ is about 0.5%. This small discrepancy can be attributed to the undulations on the $\theta_i(t)$ curves as shown in fig. 4(a). In the formation of the uniform rotation, the initial kinetic energy input on the disturbed particle is ultimately transferred to all the other particles. In this process, both the energy and the angular momentum are conserved, as confirmed in simulations. Note that in the limit of $N \rightarrow \infty$, the mean kinetic energy on each particle becomes negligibly small. As such, the emergence of the global rotation is a finite-size effect. The motion of the particles for the duration of $\Delta t/\tau_0 = 1000$ ($\lambda_D = 1$ and $\Gamma = 1$) is recorded in a movie (see the Supplemental Information).

The irregular undulations on the displacement curves in fig. 4(a), which are referred to as noise in the following discussions, are persistent during the entire simulation up to $t/\tau_0 = 1000$. Systematic simulations at varying levels of the initial disturbance and with different number of particles show that the presence of noise on the $\theta_i(t)$ -curve is a common feature in the driven motion of particles. In other words, the initial disturbance on the single particle cannot be fully transformed to a perfectly uniform rotation of the system. Here, we remark that this phenomenon bridges the dynamical and statistical aspects of the interacting particle system. While the dynamics of the interacting particles is deterministic, the noise arising on the displacement curve originates from

the randomization of particle speed under collisions. This is a spontaneous physical process that is governed by the fundamental mechanical and statistical laws. As such, the noise in the motion of particles is an intrinsic property of interacting particle systems. Note that the noise may also be interpreted as the superposition of dynamical modes, and the uniform rotation represents the fundamental zero mode.

Is there any statistical regularity underlying the noise? Especially, how could the range of interaction influence the statistical behavior of the noise? These inquiries lead us to perform statistical analysis of the trajectories of motion. Specifically, we compute the standard deviation $\delta\theta(t)$ of the instantaneous particle configuration, and then take time average of $\delta\theta(t)$, which is denoted as $\langle \delta\theta \rangle$. The information of particle-particle interaction is encoded in the quantity of the noise amplitude $\langle \delta\theta \rangle$. Analyzing $\langle \delta\theta \rangle$ allows us to explore the connection of the range of interaction and the random dynamics.

The dependence of $\langle \delta\theta \rangle$ on the screening length λ_D and the disturbance strength Γ is shown in fig. 4(c) and 4(d). From fig. 4(c), we see the abrupt reduction of $\langle \delta\theta \rangle$ with the increase of the screening length, indicating that the noise amplitude is significantly suppressed under long-range interaction. The coincidence of the curves for the different number of particles indicates that the amplitude of noise is independent of the number of particles. The noise level is also suppressed under weaker initial disturbance as shown in the plot of $\langle \delta\theta \rangle$ versus Γ in fig. 4(d). Extrapolation of the curves in fig. 4(d) to the larger λ_D regime suggests that the noise in the displacement curve would be further reduced in the Coulomb interacting systems.

D. Dynamics of speed relaxation

In this section, we discuss the dynamical process of speed redistribution among the particles. To accelerate this process, all of the particles are disturbed. The initial speed of each particle is a uniform random value in the range of $[-\Gamma_m, \Gamma_m]$. We work in the rotating frame of reference where the total angular momentum is zero. It is found that, regardless of the range of interaction, collisions of particles ultimately lead to a stable speed distribution in the form of

$$f_0(v) = Ae^{-v^2/v_p^2}, \quad (3)$$

where A is the normalization coefficient. Equation (3) is essentially the one-dimensional Maxwell-Boltzmann distribution. In fig. 5(a)-5(d), we show the typical instantaneous speed distributions in the relaxation process for $\lambda_D = 1$. The red dashed fitting curve in fig. 5(d) has the functional form of eq.(3). For the case of the single-particle driven motion, the speed distribution also evolves towards the equilibrium distribution as in eq.(3); the relaxation time for the system of $\lambda_D = 1$ and $\Gamma = 1$ is several hundred times of the characteristic time τ_0 . Here, it is of interest to note that, as a statistical law, collisions could lead to the concentration of kinetic energy on a small number of particles with high speed in the equilibrium state; any particle in the ring system has the chance of becoming the high-speed one.

To quantitatively characterize the dynamics of speed relaxation, we propose the quantity δf^2 defined as:

$$\delta f^2 = \frac{\sum_{v_i} (f(v_i) - f_0(v_i))^2}{\sum_{v_i} f_0(v_i)^2}, \quad (4)$$

where $f(v)$ is the numerically obtained instantaneous

speed distribution during the relaxation process, and $f_0(v)$ is the equilibrium speed distribution. Figures 5(e)-5(h) show the temporal variation of δf^2 at varying screening length. We see that the relaxation time significantly reduces from about $3\tau_0$ [see fig. 5(e)] to a fraction of τ_0 [see figs. 5(f)- 5(h)] with the increase of λ_D . Besides the fast relaxation process, the fluctuation of the $\delta f^2(t)$ curve seems exhibiting some degree of periodicity in the long-range interacting system of $\lambda_D = 5$ in fig. 5(h), implying the presence of some ordered dynamical structure.

IV. CONCLUSION

In summary, we investigated the dynamical response of the system to the disturbance imposed on a single particle, and reveal the featured dynamics brought by the long-range interaction. Specifically, we highlight the efficient transformation of the disturbance into the uniform global rotation of the system, the suppression of the intrinsic noise, and the fast relaxation of particle speed under the long-range interaction. These results advance our understanding on the dynamical effects of long-range interaction. The simple 1D ring model may be employed to address the fundamental questions on the interface of microscopic dynamics and statistical physics of long-range interacting systems.

Acknowledgments

This work was supported by the National Natural Science Foundation of China (Grants No. BC4190050). The author acknowledges the support from the Student Innovation Center at Shanghai Jiao Tong University.

-
- [1] D. Lynden-Bell, R. Wood, and A. Royal, *Monthly Notices of the Royal Astronomical Society* **138**, 495 (1968).
 - [2] T. Padmanabhan, *Phys. Rep.* **188**, 285 (1990).
 - [3] M. Joyce and T. Worrakitpoonpon, *Physical Review E* **84**, 011139 (2011).
 - [4] J. Lighthill, *SIAM Rev* **18**, 161 (1976).
 - [5] S. Chattopadhyay and X.-L. Wu, *Biophys. J.* **96**, 2023 (2009).
 - [6] M. C. Dallaston, M. A. Fontelos, D. Tseluiko, and S. Kalliadasis, *Phys. Rev. Lett.* **120**, 034505 (2018).
 - [7] D. A. Walker, B. Kowalczyk, M. Olvera de la Cruz, and B. A. Grzybowski, *Nanoscale* **3**, 1316 (2011).
 - [8] H. Christodoulidi, C. Tsallis, and T. Bountis, *Europhys. Lett.* **108**, 40006 (2014).
 - [9] R. Juhász, I. A. Kovács, and F. Iglói, *Europhys. Lett.* **107**, 47008 (2014).
 - [10] V. Jadhao, Z. Yao, C. K. Thomas, and M. Olvera de la Cruz, *Phys. Rev. E* **91**, 032305 (2015).
 - [11] A. Mauri and M. I. Katsnelson, *Ann. Phys.* **412**, 168016 (2019).
 - [12] Z. Yao, *Phys. Rev. Lett.* **122**, 228002 (2019).
 - [13] C. Holm, P. Kékicheff, and R. Podgornik, *Electrostatic Effects in Soft Matter and Biophysics* (Springer, Berlin, 2001).
 - [14] Y. Levin, *Rep. Prog. Phys.* **65**, 1577 (2002).
 - [15] R. Messina, *J. Phys.: Condens. Matter* **21**, 113102 (2008).
 - [16] X. Xing, *Physical Review E* **83**, 041410 (2011).
 - [17] Z. Yao and M. Olvera de la Cruz, *Phys. Rev. Lett.* **116**, 148101 (2016).
 - [18] C. Gao, S. Kewalramani, D. M. Valencia, H. Li, J. M. McCourt, M. Olvera de la Cruz, and M. J. Bedzyk, *Proceedings of the National Academy of Sciences* **116**, 22030 (2019).
 - [19] F. Bouchet and J. Barre, *J. Stat. Phys.* **118**, 1073 (2005).
 - [20] Y. Levin, *Physica A: Statistical Mechanics and its Applications* **352**, 43 (2005).
 - [21] T. Rocha Filho, A. Figueiredo, and M. A. Amato, *Phys. Rev. Lett.* **95**, 190601 (2005).
 - [22] A. Pluchino, A. Rapisarda, and C. Tsallis, *Europhys. Lett.* **80**, 26002 (2007).
 - [23] G. Joyce, G. Knorr, and H. K. Meier, *J. Comput. Phys.*

- 8, 53 (1971).
- [24] R. Pakter and Y. Levin, *J. Stat. Mech: Theory Exp.* **2017**, 044001 (2017).
- [25] L. J. Cirto, A. Rodríguez, F. D. Nobre, and C. Tsallis, *Europhys. Lett.* **123**, 30003 (2018).
- [26] J. Toner and Y. Tu, *Phys. Rev. Lett.* **75**, 4326 (1995).
- [27] R. Zhang, P. Jha, and M. Olvera de la Cruz, *Soft Matter* **9**, 5042 (2013).
- [28] B. A. Grzybowski, C. E. Wilmer, J. Kim, K. P. Browne, and K. J. Bishop, *Soft Matter* **5**, 1110 (2009).
- [29] L. P. Kadanoff, *From Order to Chaos II* (World Scientific, 1999).
- [30] F. F. Chen, *Introduction to plasma physics* (Springer Science & Business Media, 2012).
- [31] S. Rützel, S. I. Lee, and A. Raman, *Proc. R. Soc. London, Ser. A* **459**, 1925 (2003).
- [32] A. Campa, T. Dauxois, D. Fanelli, and S. Ruffo, *Physics of Long-Range Interacting Systems* (Oxford University Press, Oxford, UK, 2014).
- [33] L. Boltzmann, *Lectures On Gas Theory* (University of California Press, Berkeley, 1964).
- [34] D. Rapaport, *The Art of Molecular Dynamics Simulation* (Cambridge University Press, Cambridge, UK, 2004).
- [35] M. Feix and P. Bertrand, *Transp. Theory Stat. Phys.* **34**, 7 (2005).
- [36] Y. Sota, O. Iguchi, M. Morikawa, T. Tatekawa, and K.-i. Maeda, *Phys. Rev. E* **64**, 056133 (2001).
- [37] Y. Sokolov, D. Frydel, D. G. Grier, H. Diamant, and Y. Roichman, *Phys. Rev. Lett.* **107**, 158302 (2011).
- [38] H. Nagar and Y. Roichman, *Phys. Rev. E* **90**, 042302 (2014).
- [39] I. Williams, E. C. Oğuz, T. Speck, P. Bartlett, H. Löwen, and C. P. Royall, *Nat. Phys.* **12**, 98 (2016).
- [40] P. Debye, *Physikalische Zeitschrift* **24**, 185 (1923).
- [41] A. Dobrynin and M. Rubinstein, *Prog. Polym. Sci.* **30**, 1049 (2005).
- [42] F. Scheck, *Mechanics: from Newton's Laws to Deterministic Chaos* (Springer Science & Business Media, 2010).